Earth and Planetary Science Letters 456 (2016) 16–25

Contents lists available at ScienceDirect

Earth and Planetary Science Letters

www.elsevier.com/locate/epsl

How temperature-dependent elasticity alters host rock/magmatic reservoir models: A case study on the effects of ice-cap unloading on shallow volcanic systems

Richard R. Bakker [a,b,*], Marcel Frehner [b], Matteo Lupi [b,c]

[a] Delft University of Technology, Faculty of Civil Engineering and Geosciences, Building 23, Stevinweg 1, 2628 CN Delft, The Netherlands
[b] ETH Zurich, Geological Institute, Sonneggstrasse 5, 8092 Zurich, Switzerland
[c] University of Geneva, Department of Earth Sciences, Rue des Maraîchers 13, 1205 Geneva, Switzerland

ARTICLE INFO

Article history:
Received 18 February 2016
Received in revised form 8 September 2016
Accepted 23 September 2016
Available online xxxx
Editor: T.A. Mather

Keywords:
volcanic unloading
pressure change
transition zone around magma chamber
finite-element modelling

ABSTRACT

In geodynamic numerical models of volcanic systems, the volcanic basement hosting the magmatic reservoir is often assumed to exhibit constant elastic parameters with a sharp transition from the host rocks to the magmatic reservoir. We assess this assumption by deriving an empirical relation between elastic parameters and temperature for Icelandic basalts by conducting a set of triaxial compression experiments between 200 °C and 1000 °C. Results show a significant decrease of Young's modulus from ~38 GPa to less than 4.7 GPa at around 1000 °C. Based on these laboratory data, we develop a 2D axisymmetric finite-element model including temperature-dependent elastic properties of the volcanic basement.

As a case study, we use the Snæfellsjökull volcanic system, Western Iceland to evaluate pressure differences in the volcanic edifice and basement due to glacial unloading of the volcano. First, we calculate the temperature field throughout the model and assign elastic properties accordingly. Then we assess unloading-driven pressure differences in the magma chamber at various depths in models with and without temperature-dependent elastic parameters. With constant elastic parameters and a sharp transition between basement and magma chamber we obtain results comparable to other studies. However, pressure changes due to surface unloading become smaller when using more realistic temperature-dependent elastic properties. We ascribe this subdued effect to a transition zone around the magma chamber, which is still solid rock but with relatively low Young's modulus due to high temperatures. We discuss our findings in the light of volcanic processes in proximity to the magma chamber, such as roof collapse, dyke injection, or deep hydrothermal circulation. Our results aim at quantifying the effects of glacial unloading on magma chamber dynamics and volcanic activity.

1. Introduction

Decompression of magmatic reservoirs can be caused by crystallization (Blundy et al., 2006), un-roofing (Manconi et al., 2009; Pinel and Albino, 2013), passive degassing (Girona et al., 2014), or unloading of confining tectonic stress (Walter and Amelung, 2007). Similarly, removal of overburden may promote volcanic eruptions by reducing the lithostatic load acting on a magmatic reservoir. This effect can for example be caused by deglaciation (e.g., Pagli and Sigmundsson, 2008) and flank collapse (e.g., Manconi et al., 2009). A more direct response to load removal may occur in active or dormant volcanoes. It was previously suggested that a surface unloading of 40 bar (due to flank collapse) results in a pressure decrease of 5 to 6 bar within a magma chamber storage zone at depths of 18–22 km (Manconi et al., 2009). While some recent studies have investigated the effects of ice-cap retreat on shallow magmatic bodies (e.g., Albino et al., 2010; Manconi et al., 2009), to the best of our knowledge the effects on the upper mantle are still not investigated. Schmidt et al. (2013) suggested that unloading (due to ice-cap retreat) may also affect the upper mantle by inducing lithospheric relaxation and enhancing decompression-induced melting over timescales of hundreds to thousands of years. However, major uncertainties are still to be quantified. These are for instance the geometry of the magmatic reservoir and the lack of temperature-dependent measurements of the elastic parameters used to model such systems. As a result,

* Corresponding author at: Delft University of Technology, Faculty of Civil Engineering and Geosciences, Building 23, Stevinweg 1, 2628 CN Delft, The Netherlands.
E-mail address: R.R.Bakker@tudelft.nl (R.R. Bakker).

http://dx.doi.org/10.1016/j.epsl.2016.09.039
0012-821X/

magmatic systems are often modelled with the major assumption that the crust is isotropic and homogeneous with constant elastic properties.

In studies of time-dependent deformation of volcanic systems, temperature is typically considered an important parameter by employing a visco-elastic approach (e.g., Del Negro et al., 2009; Gregg et al., 2012; Parks et al., 2015). The rheology of the crust is modelled as a generalised Maxwell body with parallel spring-dashpot systems, whereas temperature affects the viscous response of the material (dashpot), but not the elastic (spring) part. This practice might not reflect the real elastic properties of the crust accurately. In particular, it ignores the temperature-dependence of elastic parameters (e.g., Anderson et al., 2013), especially when partial melts are considered (e.g., Kohlstedt and Zimmerman, 1996). Several studies have shown that bulk-rock elastic parameters vary significantly with temperature, especially above 600 °C (e.g., basalt: Violay et al., 2012; andesite: Smith et al., 2009; microgabbro: Violay et al., 2015; limestone: Bakker et al., 2015). Hence, neglecting the temperature-dependence of elastic properties, especially in volcanic and hydrothermal environments, may result in misleading conclusions. Gregg et al. (2012) did apply a temperature-dependency to the elastic part of the system to investigate the effects of magma over-/under-pressure, by using lowered Young's modulus at $T > 650$ °C.

The goal of our study is to compare models of a volcanic system using both temperature-dependent and temperature-independent elastic properties and hence to quantify the effect of temperature-dependency of the elastic properties. The innovative aspect of the present study is that we feed our numerical model with measured temperature-dependent elastic properties. As an application, we model pressure changes due to removal of a surface load. To provide a realistic case-study we consider a deglaciation scenario: the Snæfellsjoküll volcanic system, Iceland, whose ice cap is thinning at a rate of 1.25 m/yr on average (Jóhannesson et al., 2003).

The manuscript is structured as follows. First, we describe the Snæfellsjoküll volcanic system and describe how we sampled lithologies representative of Iceland. Next, we describe our experiments to characterise the pressure- and temperature-dependent elastic properties of the crust. The elastic properties are based on triaxial deformation experiments on basaltic lavas and hyaloclastite (i.e., hydrated tuff-like breccia) samples tested under elevated confining pressure, P (a proxy to depth), and temperature, T (depth/proximity to magma chamber), conditions appropriate for a shallow magmatic system. We then introduce the thermo-mechanical numerical model where we use the acquired laboratory data. The model quantifies the variation of stresses and pressure at crustal depths induced by ice-cap removal (i.e., we consider the thickness of the ice cap covering the Snæfellsjoküll volcanic system). We finally discuss our results and draw the main conclusions.

2. Methods

The Snæfellsjökull central volcano, like most of the Icelandic stratovolcanoes, consists of alternating layers of Tertiary basement and hyaloclastites (Alfredsson et al., 2013; Kokfelt et al., 2009). Unfortunately, the basement geology is mostly only constrained by surface observations (Tibaldi et al., 2013) and only recent studies began to investigate the volcanic system with geophysical methods (Obermann et al., 2016). Based on Tibaldi et al. (2013), we assume the Tertiary basalts to best represent the basement of the Snæfellsjökull volcanic complex and assume that hyaloclastite layers are only present in the shallow part (i.e., the volcanic edifice). The deep parts of the Snæfellsjökull volcanic system (Fig. 1) are not accessible and are therefore represented by Tertiary lavas that form the basement (Tibaldi et al., 2013). The Tertiary basement samples without significant surface alteration used in this study

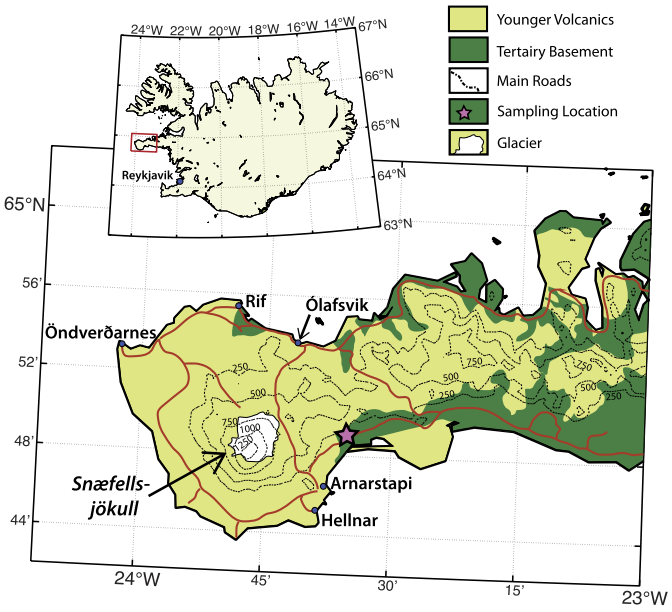

Fig. 1. Simplified geological map of the Snæfellsness peninsula (after Jóhannesson, 2009). For a coloured version of this figure we refer to the online version of this work.

were sampled from outcrops as close as possible to the volcanic edifice (Fig. 1). Samples comprise hydrothermally altered basalt with clinopyroxene (augite) and plagioclase phenocrysts in a fine-grained crystalline (glass-free) matrix with saponite and chlorite as alteration products. The material has a density of 2750 ± 50 kg m^{-3} and a connected porosity of 4.14 ± 0.02%, measured using a helium pycnometer (Micrometrics® Accupyc 1330). We measured the chemical composition using X-ray Fluorescence (XRF) techniques, which showed 4.344% loss on ignition (LOI) likely due to water released from hydrous minerals, which formed by hydrothermal alteration. For comparison, a basaltic lava flow from a recent eruption did not reveal measurable water content based on LOI (see supplementary material, Table S-2 for further details). Hyaloclastite samples used in this study consist of poorly consolidated hydrated basaltic glass spheroids with an average grain size of 0.5 mm. The samples had an initial density of 1510 ± 10 kg m^{-3} and a connected porosity of 40.01 ± 0.02%. No suitable outcrop of hyaloclastite was found in relative close proximity to the summit, nor is there comprehensive data available on the elastic properties of this rock. Therefore, samples were obtained from a roadside outcrop in the Hellisheiði volcanic field with similar chemical properties (oxides, see Table S-2). These samples are not compacted due to overburden, thus do not strictly represent deeper hyaloclastite layers (Jaya et al., 2010). To account for this caveat, we compacted the samples before experimental deformation by applying a hydrostatic confining pressure.

2.1. Rock deformation experiments

We drilled cylindrical samples (12 mm diameter, 30 mm long) from blocks of the Tertiary basalts (former lava flows) and hyaloclastite and cut them to plane-parallel end faces. Before experiments, we oven-dried the samples at 70 °C for a minimum of 24 h to ensure a dry starting material. Samples were jacketed and placed in a Paterson-type triaxial deformation apparatus. Samples were initially subjected to a hydrostatic stress (argon gas pressure) and subsequently heated to the desired temperature. Finally, axial deformation is imposed by driving up a piston, maintaining a constant strain rate, while the piston displacement and axial load is measured (see Bakker et al., 2015, for further details). Experi-

ments took place at temperatures ranging from 200 °C to 1000 °C and confining pressures from 50 MPa to 150 MPa, corresponding to approximately 2–6 km depth. During all tests, we maintained a constant strain rate of 10^{-5} s^{-1}. For each temperature, we calculated the static Young's modulus from the linear-elastic section of the stress–strain curve, in this case between 0.2 and 0.6% strain (Figs. 3 and 4). These two limits allow avoiding non-linear stress–strain effects due to closure of cracks in the sample (lower limit) or sample yielding (upper limit) (Bakker et al., 2015; Heap et al., 2009). The slope of the linear regression of the data between these limits is taken as the static Young's modulus. Deformation beyond the elastic range is measured to infer macroscopic mechanical behaviour (brittle/ductile).

It is advantageous to provide a smooth function for the temperature-dependent Young's modulus to the numerical model, avoiding sharp unnatural transitions. Therefore, we used a continuous function to represent the temperature-Young's modulus data pairs, which however reproduces the key features of the laboratory data. As the Young's modulus, E, decreases continuously with temperature but drops significantly above a threshold temperature, T_c, we used a combination of a linear function and the error function (erf):

$$E(T) = a \cdot \left[1 - \mathrm{erf}\left(\frac{T - T_c}{s}\right)\right] + b \cdot T + c, \quad (1)$$

where $E(T)$ is the temperature-dependent Young's modulus and T_c is the threshold temperature at which the Young's modulus decreases by an order of magnitude or more. Parameters a, b, c, s, and T_c are fitting parameters.

Prior to axial deformation, the hyaloclastite samples were hydrostatically compacted by the confining pressure. As a result, the cross-sectional area and length of the sample changed significantly before axial deformation commenced. Therefore, the imposed compaction prior to the deformation experiment could only be assessed post-testing, resulting in uncertain axial stresses used to calculate Young's moduli. For this reason, these data are averaged, and treated as indicative values without any temperature-dependence. A more comprehensive study on the compaction behaviour of hyaloclastite is required.

We could not measure the Poisson's ratio because there is insufficient space between the sample and the inner furnace wall to mount a radial LVDT (linear variable displacement transducer) or strain gauge (e.g., Heap et al., 2009). In addition, the jacketing material is electrically conductive, making it impossible to create an isolated electrical circuit. However, previous studies indicate that the Poisson's ratio does not change dramatically with varying P/T conditions as long as the material is solid and is not prone to (partial) melting (Christensen, 1996; Tarkov and Vavakin, 1982). Therefore, not knowing this parameter is unlikely to influence the temperature-dependent model presented here.

When rocks are exposed to sufficient temperatures, their rheological behaviour changes from brittle to ductile. Therefore, we assume the Poisson's ratio, ν, to increase with temperature from $\nu_{min} = 0.25$ to $\nu_{max} = 0.49$. The lower value is commonly found in uniaxial testing of basalts (Christensen, 1996); the upper value corresponds to a near-incompressible visco-elastic case, where rocks have a high bulk-to-shear modulus-ratio (Greaves et al., 2011). The Poisson's ratio is scaled to the normalised Young's modulus as

$$\upsilon(T) = \left[1 - \frac{E(T)}{E_{max}}\right] \cdot [\upsilon_{max} - \upsilon_{min}] + \upsilon_{min}. \quad (2)$$

The inverse relationship between Young's modulus and Poisson's ratio is also qualitatively shown by Heap et al. (2009). However, in Heap et al. (2009) the decrease in Young's modulus is due to an increase in damage caused by cyclic stressing of samples and not by temperature, as in the present study.

2.2. Finite-element modelling setup

Similar to Manconi et al. (2009) and Albino et al. (2010), we employ a two-dimensional axisymmetric finite-element model. We approximate the topography of the Snæfellsjökull volcano by a Gaussian function with 0 m elevation at the edge of the model and the maximum height corresponding to the volcano's summit at 1446 m. The ice cap is assumed to have its maximum thickness at the top of the volcano and decreases in thickness down to zero at the volcano's half width. For this thickness distribution we use a similar Gaussian function, with 0 thickness on the edges and its maximum thickness in the middle, above the volcano's summit. In the model, the width of the resulting ice cap can be varied, but is chosen to correspond to the current extent of Snæfellsjökull's ice cap (modelled at 8 km in diameter). The current maximum thickness is around 110 m and mean thickness around 30 m (and decreasing) (Björnsson and Pálsson, 2008). However, estimates for glacier thickness during the last glacial maximum vary between 300 and 500 m (Biessy et al., 2008). The stratigraphic nature of the volcano is reproduced by a layered setup, with alternating layers of lava flows and hyaloclastite, typical of Icelandic central volcanoes (Alfredsson et al., 2013).

We adapted a finite-element model to solve the steady-state thermal conduction–advection equations, as well as the force balance and linear elastic rheological equations. For symmetry reasons, we approximate the geometry of the Snæfellsjökull volcano by a 2D axisymmetric half-space (Fig. 2). In most model runs the horizontal extent is set to 10 km (corresponding to a diameter of 20 km). The vertical extent is set from 1446 m a.s.l. (current maximum elevation of Snæfellsjökull) to 15 km depth, which captures the depth of the Icelandic crust (Björnsson, 2008). In Iceland, the depth of the brittle–ductile transition is assumed to occur between 10 and 15 km depth (Stefansson et al., 2008). The magmatic reservoir, approximated as an elliptical magma chamber, is situated at 5 km depth providing enough space below to prevent boundary effects. Icelandic volcanic systems are often characterised by shallow magma chambers (Andrew and Gudmundsson, 2008 and references therein).

The calculations take place in three steps. At the first step, the thermal conduction–advection equations are solved. The boundary conditions are:

- 0 °C within the ice cap;
- 1200 °C within the magma chamber and at the bottom boundary of the model;
- Zero horizontal heat flux across the symmetry axis (left boundary in Fig. 2);
- Zero horizontal heat flux across the outer model boundary (right boundary in Fig. 2).

To simulate the presence of a hydrothermal system above the magma chamber, we apply a simple advection term in vertical direction. Advection velocities greatly depend on the large-scale permeability of the system (e.g., Scott et al., 2015) and are therefore poorly constrained. We chose the advection term such that the surface temperature gradients correspond to values measured in boreholes in volcanic fields (e.g., Björnsson, 2008; Flóvenz and Saemundsson, 1993; Scott et al., 2015). Based on the obtained steady-state temperature field, we assign the measured temperature-dependent elastic parameters (Young's modulus and Poisson's ratio; Equations (1) and (2)) to each element in the model.

In the second step of our modelling procedure, the force balance and linear elastic rheological equations are solved to obtain the pressure field in the model under the effect of gravity. The following boundary conditions apply:

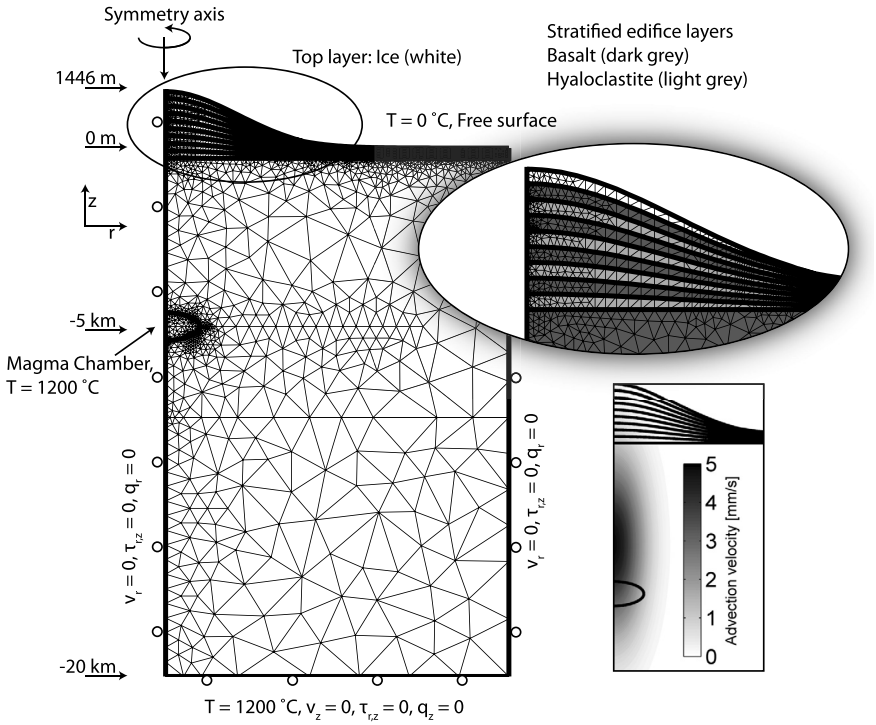

Fig. 2. Numerical model setup of the 2D axisymmetric half-space with all applied boundary conditions. Used abbreviations: r and z, radial and depth coordinates (or when used as subscripts: directions); v, displacement; τ, shear stress; q, heat flux; T, temperature. Roller boundary conditions are indicated by circles. The shown numerical mesh is simplified as the true mesh is too dense to be depicted here. Inset shows the advection velocity field with values ranging from 0 to 5 mm/s. Note that the depth of the magma chamber and depth of the model are variable, noted here are those for the reference state, at 5 and 20 km b.s.l., respectively.

- Zero traction along the symmetry axis (left boundary in Fig. 2);
- Zero traction along the outer (right boundary in Fig. 2) and bottom model boundaries;
- Free surface boundary at the top of the model.

Initial testing revealed that the load of the volcano is sufficiently far away from the outer model boundary such that the model size does not influence the result. Material properties are listed in the supplementary material: Table S-1. For temperature-dependent models, the Young's modulus and Poisson's ratio for basalt and magma are overwritten by Equations (1) and (2), respectively.

The third step repeats the previous step, but without an ice cap. The pressure difference between the third and second step corresponds to the pressure change when the ice cap is removed. As this approach is purely elastic, it is time-independent; hence visco-elastic or plastic effects are neglected.

The details of the finite-element model are beyond the scope of this work as other implementations of the same numerical code have successfully been benchmarked and verified elsewhere providing full technical details (e.g., Tuitz et al., 2012; Zhong et al., 2014 and references therein). Uncertainties in the model result due to uncertainties in elastic parameters have been assessed during feasibility testing. Absolute pressures (not pressure differences) were within 0.3 bar when systematically varying the Young's modulus of the basement by ±2 GPa (far more than the experimental error) and Poisson's ratio between 0.1 and 0.4.

3. Results

3.1. Triaxial deformation

The results of our deformation experiments are first evaluated as a whole by means of their stress–strain curves, followed by a focus on the elastic part thereof. Experiments at a constant confining

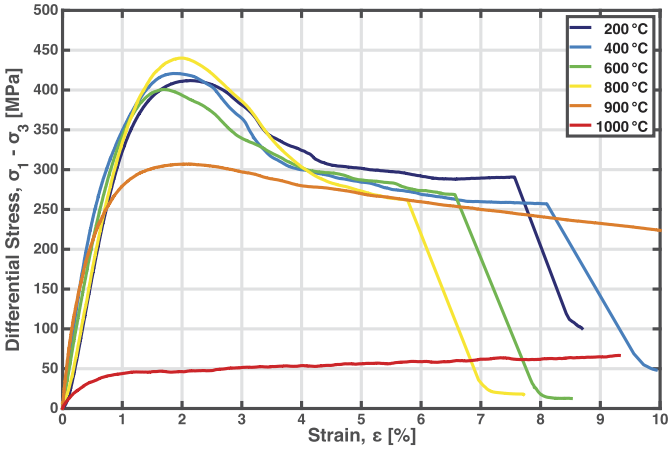

Fig. 3. Differential stress-versus-strain curves for hydrothermally altered basalt samples. Experiments were conducted at a confining pressure of 50 MPa, a constant strain rate of 10^{-5} s^{-1}, and varying temperatures. For a coloured version of this figure we refer to the online version of this work.

pressure (P_c) of 50 MPa and strain rate, but varying temperatures (Fig. 3) can be classified as follows. At temperatures up to and including 800 °C, sample deformation is elastic up to ~1% strain and differential stress of ~350 MPa. Beyond this elastic limit the samples start to yield and eventually reach peak differential stress values of about 400–440 MPa at ~1.7% strain. This is followed by gradual weakening until differential stresses stabilise at ~4% strain and steady state differential stresses around 300 MPa. In all of these cases, a second significant decrease in stress occurs at strains between 6 and 8%, which is due to jacket puncture and is therefore not representative for the sample behaviour and was not included in further analysis. The experiment at 900 °C exhibits a similar elastic loading until yield at ~0.5% strain and 200 MPa differential stress. Continued deformation leads to a peak differen-

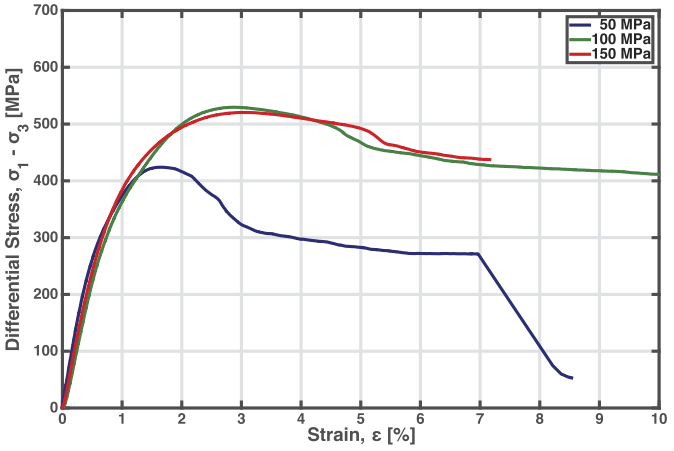

Fig. 4. Differential stress-versus-strain curves for hydrothermally altered basalt samples. Experiments were conducted at a temperature of 400 °C, a constant strain rate of 10^{-5} s^{-1}, and with varying confining pressures. For a coloured version of this figure we refer to the online version of this work.

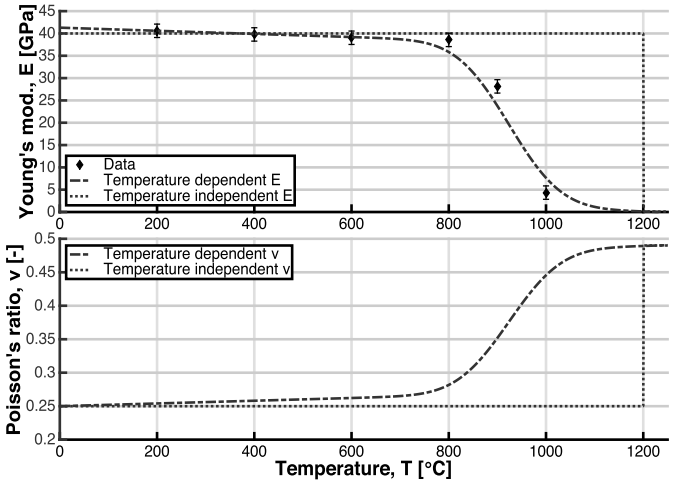

Fig. 5. Young's modulus (GPa) and Poisson's ratio (−) vs. temperature (°C). The Young's modulus data points result from laboratory triaxial shortening experiments, which are fitted with a continuous function (Equation (1)). The Poisson's ratio is calculated using a similar function as for the Young's modulus (Equation (2)).

tial stress of 310 MPa at ∼2% strain, followed by a weakening until 10% strain, after which the experiment was concluded. At 1000 °C, a short pseudo-linear deformation phase occurs up to ∼0.5% strain, followed by a slight strengthening.

We investigated the effect of confining pressure by deforming samples at a constant temperature of 400 °C and strain rate, but varying confining pressures of 50, 100, and 150 MPa. All samples started to yield at ∼1% strain. However, while the experiment at a confining pressure of 50 MPa reached a peak differential stress of 420 MPa at ∼1.7% strain, the samples deformed at 100 and 150 MPa confining pressure exhibited a peak differential stress of 530 MPa at around ∼3% strain. Continued deformation led to a phase of gradual weakening, followed by a slight stress decrease at around 5% strain for the 100 and 150 MPa experiments. Continuous deformation did not result in jacket puncture as with the 50 MPa experiment. However, these experiments were concluded to avoid high pressure leaks, as well as avoiding non-homogeneous stress distribution within the sample (e.g., Paterson and Wong, 2005).

During the elastic part of deformation (i.e., 0.2–0.6% strain), the triaxial experiments on Snæfellsjökull basalt revealed no significant influence of confining pressure on Young's modulus. Results of experiments at 50 MPa, 100 MPa, and 150 MPa confining pressure lie within experimental error (Fig. 4). Between 200 °C and 800 °C, the Young's modulus linearly decreases from 41 to 38 GPa. Beyond that, the Young's modulus sharply drops to 24 GPa at 900 °C and 4.7 GPa at 1000 °C (Fig. 3). Alpha-95 confidence intervals derived from the fitting of the stress–strain curves lie within 0.2 GPa of the reported values. However, to account for a large degree of variability between samples we assume an error of 2 GPa. Above 1000 °C, the low sample strength prevented accurate measurements of differential stress.

The hyaloclastite samples exhibit an average Young's modulus of 20 ± 5 GPa, which compares well to literature data (Jaya et al., 2010). Nonetheless, our results are not accurate enough to interpret a temperature-dependency with confidence. The compacting behaviour and the effects thereof on the elastic properties of hyaloclastite may be a topic of further investigation. However, as the occurrence of these rocks is limited to the volcanic edifice, the magma chamber is unlikely residing in hyaloclastite host rock. We therefore focus on the Tertiary basalt as host rock.

The significant decrease of Young's modulus of the Tertiary basalt at high temperatures is likely associated with the transition from brittle to ductile behaviour (e.g., Bakker et al., 2015). Indeed, the samples deformed at temperatures up to 800 °C exhibited a loss of load-carrying capacity after about 2% strain (observed by the weakening after reaching peak differential stress) and analysis of the resulting microstructure revealed localised deformation (see supplementary data). Conversely, samples deformed at 900 °C and 1000 °C did not exhibit significant loss of load-carrying capacity and did not show signs of localisation in the resulting microstructure. Therefore, we interpret the brittle–ductile transition to be at 850 ± 50 °C for $P_c = 50$ MPa and a strain rate of 10^{-5} s^{-1}. Additionally, the change in behaviour is associated with a decrease in peak and yield differential stresses (Figs. 3 and 4).

With known Young's modulus (E) and Poisson's ratio (ν), the bulk modulus (K) can be calculated as $K = E/(3(1-2\nu))$. Assuming a Poisson's ratio of 0.49 (common for visco-elastic behaviour of a solid), the range of Young's moduli at >1000 °C of $E = 0.1$–5 GPa corresponds to a bulk modulus of $K = 0.006$–0.3 GPa. This compares well with the lower end of published bulk moduli of magma (0.1–10 GPa; Huppert and Woods, 2002; Tait et al., 1989). However, it should be noted that bulk modulus for magmas strongly depends on magma chamber size and overpressure (Melnik and Sparks, 2005).

Equation (1) is applied to the laboratory data of Young's modulus and Poisson's ratio as a function of temperature (see Fig. 5). The applied fitting parameters are: $a = 1.85 \times 10^{10}$, $b = -3.5 \times 10^{6}$, $c = 4.3 \times 10^{9}$, $s = 120$, and $T_c = 924$.

3.2. Finite element model results with and without temperature dependency

The calculated temperature field and resulting distributions of elastic parameters are presented in Fig. 5. Concentrating only on the magma storage zone, our numerical results suggest that the removal of an initially 200 m thick ice cap reduces the pressure in the magma chamber at 5 km depth (below sea level, b.s.l.) by ∼0.5 bar (see Fig. 6). Pressure changes do not vary significantly between models with and without imposed layering. However, this pressure change strongly depends on the depth of the magma chamber. The pressure in a magma chamber at 1 km depth b.s.l. drops by 1.4 bar compared to 0.4 bar in a magma chamber at 10 km depth b.s.l. The pressure decrease in the magma chamber due to ice-cap unloading varies linearly with the thickness of the ice cap. In addition, the size of the magma chamber influences the pressure decrease slightly; for smaller magma chambers (∼0.5 km radius) pressure changes are in the order of 1.0 bar compared to ∼0.5 bar for large magma chamber (∼5 km radius).

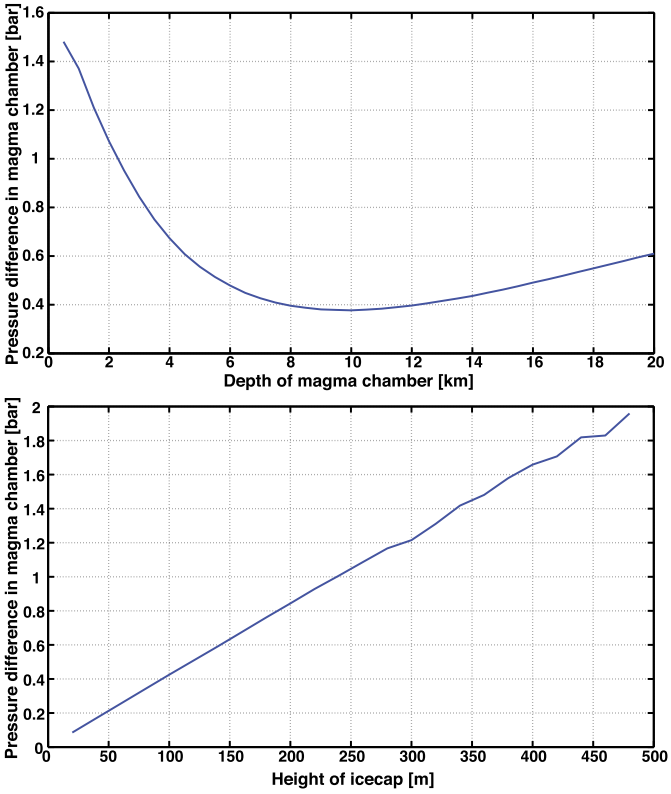

Fig. 6. Upper panel: Pressure change (bar) in the magma chamber at various depths (km) due to the removal of a 200 m thick ice cap, employing a model of 8 edifice layers. Lower panel: Pressure change (bar) in the magma chamber with various thicknesses of the ice cap (m), for a magma chamber at 3 km depth, 8 edifice layers, and a constant width of the ice sheet of 8 km.

The largest reduction in pressure occurs directly below the initial load within the volcanic edifice. The effect reaches greater depths but with decreasing magnitude. For example, removing a modelled 200 m thick ice cap reduces the pressure just below the surface by 4 bar, compared to 2 bar at 2 km depth (Figs. 8A and 8B). Interestingly, this pressure reduction is much smaller than the reduction that may be expected and approximated as $\rho gh = 18$ bar (ρ: density of ice; g: gravitational acceleration; h: thickness of removed ice). We explain this discrepancy by the self-supporting 3D geometry of the volcanic edifice (Gaussian) as opposed to a flat horizontal topography used for the approximate equation above.

In both temperature-independent and temperature-dependent models, unloading leads to an increase in pressure immediately above and below the magma chamber. This is particularly true if the horizontal extent of the unloaded mass (ice cap) is wider than the width of the magma chamber. Unloading allows regions of the rock mass originally under the surface load (i.e., the ice cap) to rebound and slightly uplift; regions further away, which did not have a surface load, to slightly subside. This surface deformation pattern is common for post-glacial rebound (e.g., Árnadóttir et al., 2009) and occurs here on a smaller scale. It is the surface expression of a rotation at depth around a pivot point (horizontal pivot line in our axisymmetric model) roughly corresponding to the edge of the removed ice-cap load. This rotational deformation causes compression towards the symmetry axis at depth, which in turn causes a pressure increase in the area where the magma chamber resides. This effect can counteract the effect of the initial unloading, as shown in Figs. 8A and 8B. However, at the outer edges of the magma chamber, pressure decreases. In the magma chamber itself pressure also decreases, but less than in the surrounding host rock (Fig. 8B).

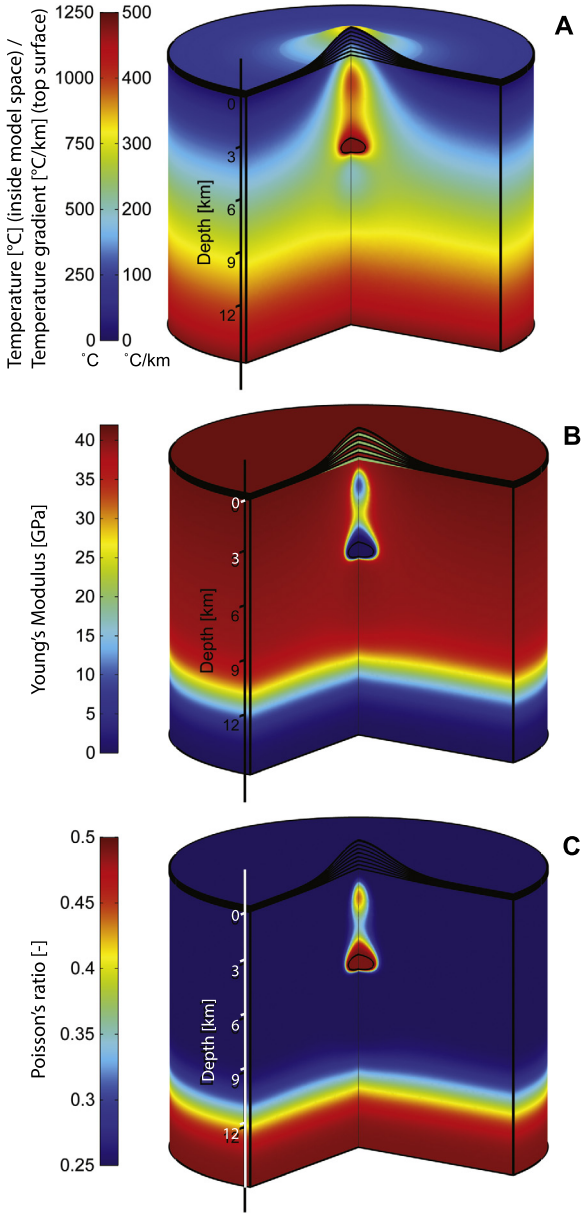

Fig. 7. 3D projected results of: A) Temperature distribution (°C) within the model space (inside volume) and surface temperature gradients (°C/km; projected on top); B) Young's modulus distribution (GPa) based on the temperature field; C) Poisson's ratio distribution (−) based on the temperature field. For a coloured version of this figure we refer to the online version of this work.

Employing a continuous temperature-dependent function for Young's modulus results in a smooth transition of mechanical parameters between the host rocks and the magma chamber (Fig. 7), compared to a sharp boundary in temperature-independent models (Fig. 5). The difference is most prominent around the magma chamber (Fig. 8). In temperature-independent models, large pressure gradients occur close to the magma chamber (Fig. 8A), compared to a more gradual pressure variation when the Young's modulus is temperature-dependent (Fig. 8B). Directly above and below the magma chamber, the two models differ as much as 2 bar (Fig. 8C). For example, in temperature-independent models the pressure increases by 1 bar directly above the magma chamber, while in temperature-dependent models there is a pressure decrease of about 0.5 bar. Furthermore, temperature-independent models exhibit a sharp pressure decrease at the outer edges of the magma chamber compared to a gradual decrease in temperature-

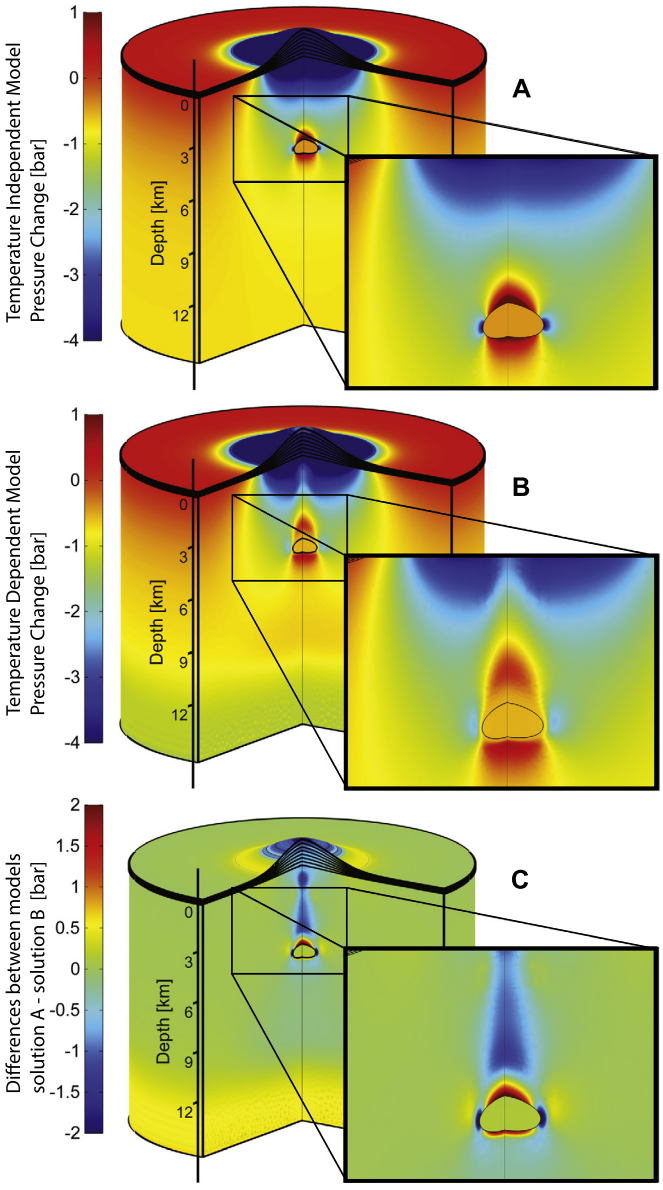

Fig. 8. 3D projected results (with zoom inset). In all cases, the models simulate the pressure changes (bar) for the removal of a 200 m thick ice cap. A) Temperature-independent model; B) Temperature-dependent model; C) Differences between the two types of models (bar). For a coloured version of this figure we refer to the online version of this work.

dependent models. Pressure changes (increase/decrease) are less extreme in temperature-dependent models, suggesting a damping effect around the magma chamber.

4. Discussion

4.1. Causes for temperature-dependent elastic properties

The distinct decrease in Young's modulus at a threshold temperature is reported for a wide range of rock types and correlates with the brittle–ductile transition. At laboratory strain rates of 10^{-5} s^{-1}, this transition occurs at 987 ± 12 °C for Etna basalt at $P_c = 50$ MPa (Bakker et al., 2015), at >800 °C for glass-free basalt at $P_{\text{eff}} = 100$ MPa (Violay et al., 2015), and at 850 ± 50 °C for Snæfellsjökull basement basalt (free of interstitial glass) at $P_c =$ 50 MPa (this study), with P_c and P_{eff} being the confining pressure and the effective pressure, respectively. Violay et al. (2012) compared the deformation behaviour of glassy and non-glassy basanite and reported that, when one component (i.e., the glass) becomes significantly weak, it controls the overall mechanical behaviour of the rock. A similar behaviour can be expected during partial melting. If sufficient melting occurs, pockets of melt can coalesce and form a melt-film network, which has been shown to cause low flow stresses (Paquet et al., 1981). The samples used in this work are characterised by hydrothermal alteration. The hydrothermally altered samples contain 4.344 wt% water, which can reduce the solidus to lower temperatures compared to dry solidus temperatures (Melnik and Sparks, 2005). Based on the chemical data presented in the supplementary material and using the method of Giordano et al. (2008), we find values of the glass transition temperature between 490 and 670 °C, depending on water content. However, in the absence of glass, the actual melting temperature may well be in the range of the brittle-to-ductile transition temperature at around $850\,°C \pm 50\,°C$ as interpreted here, even though this was neither measured directly nor reported in the literature. More testing is required to investigate the degree of partial melting at high temperatures (>900 °C, where the weakening is observed).

4.2. Broader implications of temperature-dependent elastic properties in time-independent models

The effect at depth caused by a reduction of the vertical load due to ice-sheet removal has not been quantified before using temperature-dependent elastic parameters. The large difference between temperature-dependent and temperature-independent models shows that assuming temperature-independent elastic properties for the host rock does not accurately represent the physical state of shallow magmatic systems, and should be reconsidered.

In low-temperature domains (shallow and/or at significant distance to the magma chamber), the pressure changes in the basement and in the edifice observed in this study (i.e., temperature-dependent) are comparable with previous findings (temperature-independent, Albino et al., 2010). We ascribe this to the relatively low temperatures in the brittle domain away from the magmatic reservoir, so that constant elastic properties are an adequate assumption. However, significant differences occur in close proximity to the magma chamber and at depth and close to the brittle–ductile transition. There, temperature-independent elastic properties are a poor assumption when modelling volcanic environments and regions close to the solidus in a time-independent manner.

In most previous studies, magma chambers are represented as a circle (sphere) or ellipse (ellipsoid) (e.g., Albino et al., 2010; Pinel and Albino, 2013; Sigmundsson et al., 2010), yet in nature the magma chamber is likely more complex. In our models, we also prescribe the magma chamber as an ellipse at depth, but it is only associated with a temperature boundary in the temperature-dependent models. In terms of mechanical properties, the magma chamber is essentially the same material as the basement rocks, and corresponds to a zone of low Young's modulus and high Poisson's ratio due to the imposed high temperature. Most important, the magma chamber is not defined by sharp boundaries in mechanical properties. Such sharp boundaries have been shown to act as stress concentrators and can affect stress paths (e.g., Andrew and Gudmundsson, 2008). Previous work has already highlighted the significance of considering a "ductile aureole", or transition zone, around a magma chamber, noting that it effectively has a dampening effect between magma chamber and host rocks (Parks et al., 2015). Parks et al. (2015) used a visco-elastic shell approach to model this ductile aureole. Here, the soft transition zone around the magma chamber is achieved by temperature-dependent elastic properties and corresponds to a zone with relatively low Young's modulus compared to the surrounding regions away from the magmatic reservoir. As a result, pressure changes due to unloading are less extreme in temperature-dependent mod-

els than in temperature-independent models. This implies that the temperature-dependence of elastic properties is of particular importance when investigating processes in proximity of ductile domains (Fig. 8). The fact that in temperature-dependent models the pressure changes are damped (i.e., less extreme pressure differences) has important implications for the understanding of magmatic processes. For example, dyke extrusions and the storage capacity of magmatic reservoirs are supposed to be strongly affected by the reduced lithostatic load (Hooper et al., 2011; Sigmundsson et al., 2010). Our models suggest that these processes may not be affected as dramatically as currently thought.

Our numerical solutions are time-independent representing the steady-state stress field before and after removal of the ice sheet. Since we are primarily concerned about the temperature effect on the time-independent elastic properties, laboratory-derived visco-elastic properties were not taken into account. In future studies, it would be of interest to test the time-dependent effects by using a visco-elastic approach; in other words, to evaluate what happens between our two steady-state solutions. Time-dependent visco-elastic effects could potentially be constrained by laboratory experiments where the strain rate is varied. However, such experiments would need to properly correct for the strain-hardening or -weakening effects (observed at 900 °C and 1000 °C respectively, see Fig. 3).

Within our model we treat the magma chamber as an incompressible fluid by imposing a Poisson's ratio of 0.49. In natural cases, gas can be a significant component, especially in shallow magma chambers (e.g., Degruyter and Huber, 2014; Tait et al., 1989). We have simulated this effect by systematically changing the Poisson's ratio (0.1–0.49) of the magma chamber during feasibility testing. The Poisson's ratio did not have a significant influence on the model result.

Our current understanding of magmatic processes, such as roof collapse (Browning and Gudmundsson, 2015; Tait et al., 1989), dyke initiation (e.g., Browning et al., 2015; Lister and Kerr, 1991), and dyke propagation (e.g., Gudmundsson, 2002) is largely based on models with temperature-independent elastic properties of the country rocks, and needs to be revisited.

Our findings may have important implications for future numerical studies and the understanding of various geological processes such as emplacement of magmatic bodies, effects of tectonic loads on magmatic reservoirs and effects of regional earthquakes on nearby volcanic systems. Most notably, temperature-dependent elastic properties directly affect dyking as the width of a dyke is proportional to the elastic properties of the host medium when a constant overpressure is assumed (McLeod and Tait, 1999; Rubin, 1995). Lower Young's moduli lead to wider (thicker) dykes. With realistic temperature-dependent elastic properties (i.e., a smooth transition between the magmatic reservoir and the host rocks) dykes encounter less stiff conditions when they are initiated implying that they are wider than currently estimated by temperature-independent models. The propagation velocity of a dyke is inversely proportional to the squared Young's modulus of the host rock (Rubin, 1995). Thus, a low Young's modulus close to the magma chamber causes dykes to propagate out of a magma chamber faster than previously thought. The combined effect of wider and faster propagating dykes allows greater volumes of magma to flow into the host rock surrounding the magma chamber. Furthermore, recent studies (Degruyter and Huber, 2014) indicate that the perturbation necessary to destabilise a magmatic system may be in the order of few MPa, unless the plumbing system is already in a critical state. We show that deglaciation periods can impose pressure variations in the order of 1 bar for the relatively small ice cap of Snæfellsjökull. Extrapolating to larger scales (i.e., ice thickness of 2 km, estimated for the last glacial maximum), our results are in the order of 10 bar, which is within the range of destabilising the magmatic system (Degruyter and Huber, 2014). Such pressure change may cause deglaciation-triggered melt pumping from the mantle, which in turn may replenish the shallow magmatic reservoirs. This process may be boosted by enhancement of dyking at depth, promoted by the reduced lithostatic load. This may explain the established relationship between deglaciation periods and increased volcanic activity (Glazner et al., 1999; Huybers and Langmuir, 2009; McGuire et al., 1997; Nakada and Yokose, 1992; Pagli and Sigmundsson, 2008; Robock, 2000; Watt et al., 2013).

5. Conclusions

The lack of temperature-dependence in numerical models leads to sharp transitions in elastic properties between the magmatic reservoir and the host rocks, which in itself might lead to inaccurate results. This can be improved by using temperature-dependent elastic parameters from laboratory measurements. We obtained such data for basalts from Iceland by performing triaxial deformation experiments at volcano-tectonic pressures and temperatures (50–150 MPa, 200–1000 °C). We find that increasing temperature lowers the Young's modulus, particularly above 800 °C, which we suggest to be associated with the brittle–ductile transition. We did not find any significant effects of confining pressure ($\geq$50 MPa).

Based on our laboratory data, we created a numerical model using temperature-dependent elastic properties. As a case study, we calculated pressure changes in the volcanic subsurface of the Snæfellsjökull volcano due to ice-cap removal and related surface unloading. We found that in the low-temperature domain (up to $\sim$800 °C) the temperature-dependent models correspond well with the temperature-independent models. However, close to the magma chamber, where high temperatures prevail, a transition zone exists. This reduces the magnitude of pressure changes in temperature-dependent models compared to models that use temperature-independent elastic properties. Moreover, temperature-dependent models succeed in having gradual transitions between magma and host rock and provide a more realistic picture of the state of pressure inside the volcanic edifice. Such an approach is crucial for future studies investigating processes in and around the magma chamber such as dyke extrusion and propagation or magmatic roof collapse. In the case of ice-cap retreat, temperature-dependent models may eventually lead to a better understanding of the observed increase of CO_2 after glacial maxima (Huybers and Langmuir, 2009; Watt et al., 2013).

Acknowledgements

The authors would like to thank R. Hoffman for technical assistance, J. Berger and L. Zehnder for help with petrological work, and J.-P. Burg, P.M. Benson, M.E.S. Violay, and F.M. Aben for their valuable insights. R.R.B. and M.F. acknowledge funding by the Swiss National Science Foundation, project 137867 and project 143319, respectively. M.L. acknowledge the FNSNF *Ambizione* funding scheme (project number PZ00P2_154815). This work has benefited from valuable comments by John Browning and an anonymous reviewer.

Appendix A. Supplementary material

Supplementary material related to this article can be found online at http://dx.doi.org/10.1016/j.epsl.2016.09.039.

References

Albino, F., Pinel, V., Sigmundsson, F., 2010. Influence of surface load variations on eruption likelihood: application to two Icelandic subglacial volcanoes, Grímsvötn and Katla. Geophys. J. Int. 181, 1510–1524. http://dx.doi.org/10.1111/j.1365-246X.2010.04603.x.

Alfredsson, H.A., Oelkers, E.H., Hardarsson, B.S., Franzson, H., Gunnlaugsson, E., Gislason, S.R., 2013. The geology and water chemistry of the Hellisheidi, SW-Iceland carbon storage site. Int. J. Greenh. Gas Control 12, 399–418. http://dx.doi.org/10.1016/j.ijggc.2012.11.019.

Anderson, O.L., Isaak, G., Isaak, D.G., 2013. Elastic constants of mantle minerals at high temperature. In: Mineral Physics & Crystallography: A Handbook of Physical Constants. American Geophysical Union, pp. 64–97.

Andrew, R.E.B., Gudmundsson, A., 2008. Volcanoes as elastic inclusions: their effects on the propagation of dykes, volcanic fissures, and volcanic zones in Iceland. J. Volcanol. Geotherm. Res. 177, 1045–1054. http://dx.doi.org/10.1016/j.jvolgeores.2008.07.025.

Árnadóttir, T., Lund, B., Jiang, W., Geirsson, H., Björnsson, H., Einarsson, P., Sigurdsson, T., 2009. Glacial rebound and plate spreading: results from the first countrywide GPS observations in Iceland. Geophys. J. Int. 177, 691–716. http://dx.doi.org/10.1111/j.1365-246X.2008.04059.x.

Bakker, R.R., Violay, M.E.S., Benson, P.M., Vinciguerra, S.C., 2015. Ductile flow in sub-volcanic carbonate basement as the main control for edifice stability: new experimental insights. Earth Planet. Sci. Lett. 430, 533–541. http://dx.doi.org/10.1016/j.epsl.2015.08.017.

Biessy, G., Dauteuil, O., Van Vliet-Lanoë, B., Wayolle, A., 2008. Fast and partitioned postglacial rebound of southwestern Iceland. Tectonics 27, 1–18. http://dx.doi.org/10.1029/2007TC002177.

Björnsson, A., 2008. Temperature of the Icelandic crust: inferred from electrical conductivity, temperature surface gradient, and maximum depth of earthquakes. Tectonophysics 447, 136–141. http://dx.doi.org/10.1016/j.tecto.2006.02.027.

Björnsson, H., Pálsson, F., 2008. Icelandic glaciers. Jökull 58, 365–386.

Blundy, J., Cashman, K., Humphreys, M., 2006. Magma heating by decompression-driven crystallization beneath andesite volcanoes. Nature 443, 76–80. http://dx.doi.org/10.1038/nature05100.

Browning, J., Gudmundsson, A., 2015. Surface displacements resulting from magma-chamber roof subsidence, with application to the 2014–2015 Bardarbunga–Holuhraun volcanotectonic episode in Iceland. J. Volcanol. Geotherm. Res. 308, 82–98. http://dx.doi.org/10.1016/j.jvolgeores.2015.10.015.

Browning, J., Drymoni, K., Gudmundsson, A., 2015. Forecasting magma-chamber rupture at Santorini volcano, Greece. Sci. Rep. 5, 15785. http://dx.doi.org/10.1038/srep15785.

Christensen, N.I., 1996. Poisson's ratio and crustal seismology. J. Geophys. Res. 101, 3139. http://dx.doi.org/10.1029/95JB03446.

Degruyter, W., Huber, C., 2014. A model for eruption frequency of upper crustal silicic magma chambers. Earth Planet. Sci. Lett. 403, 117–130. http://dx.doi.org/10.1016/j.epsl.2014.06.047.

Del Negro, C., Currenti, G., Scandura, D., 2009. Temperature-dependent viscoelastic modeling of ground deformation: application to Etna volcano during the 1993–1997 inflation period. Phys. Earth Planet. Inter. http://dx.doi.org/10.1016/j.pepi.2008.10.019.

Flóvenz, Ó.G., Saemundsson, K., 1993. Heat flow and geothermal processes in Iceland. Tectonophysics 225, 123–138. http://dx.doi.org/10.1016/0040-1951(93)90253-G.

Giordano, D., Russell, J.K., Dingwell, D.B., 2008. Viscosity of magmatic liquids: a model. Earth Planet. Sci. Lett. 271, 123–134. http://dx.doi.org/10.1016/j.epsl.2008.03.038.

Girona, T., Costa, F., Newhall, C., Taisne, B., 2014. On depressurization of volcanic magma reservoirs by passive degassing. J. Geophys. Res., Solid Earth, 8667–8687. http://dx.doi.org/10.1002/2014JB011368.

Glazner, A.F., Manley, C.R., Marron, J.S., Rojstaczer, S., 1999. Fire or ice: anticorrelation of volcanism and glaciation in California over the past 800,000 years. Geophys. Res. Lett. 26, 1759–1762. http://dx.doi.org/10.1029/1999GL900333.

Greaves, G.N., Greer, A.L., Lakes, R.S., Rouxel, T., 2011. Poisson's ratio and modern materials. Nat. Mater. 10, 986. http://dx.doi.org/10.1038/nmat3177.

Gregg, P.M., De Silva, S.L., Grosfils, E.B., Parmigiani, J.P., 2012. Catastrophic caldera-forming eruptions: thermomechanics and implications for eruption triggering and maximum caldera dimensions on Earth. J. Volcanol. Geotherm. Res. 241–242, 1–12. http://dx.doi.org/10.1016/j.jvolgeores.2012.06.009.

Gudmundsson, A., 2002. Emplacement and arrest of sheets and dykes in central volcanoes. J. Volcanol. Geotherm. Res. 116, 279–298. http://dx.doi.org/10.1016/S0377-0273(02)00226-3.

Heap, M.J., Vinciguerra, S., Meredith, P.G., 2009. The evolution of elastic moduli with increasing crack damage during cyclic stressing of a basalt from Mt. Etna volcano. Tectonophysics 471, 153–160. http://dx.doi.org/10.1016/j.tecto.2008.10.004.

Hooper, A., Ófeigsson, B., Sigmundsson, F., Lund, B., Einarsson, P., Geirsson, H., Sturkell, E., 2011. Increased capture of magma in the crust promoted by ice-cap retreat in Iceland. Nat. Geosci. 4, 783–786. http://dx.doi.org/10.1038/ngeo1269.

Huppert, H.E., Woods, A.W., 2002. The role of volatiles in magma chamber dynamics. Nature 420, 493–495. http://dx.doi.org/10.1038/nature01211.

Huybers, P., Langmuir, C., 2009. Feedback between deglaciation, volcanism, and atmospheric CO_2. Earth Planet. Sci. Lett. 286, 479–491. http://dx.doi.org/10.1016/j.epsl.2009.07.014.

Jaya, M.S., Shapiro, S.A., Kristinsdóttir, L.H., Bruhn, D., Milsch, H., Spangenberg, E., 2010. Temperature dependence of seismic properties in geothermal rocks at reservoir conditions. Geothermics 39, 115–123. http://dx.doi.org/10.1016/j.geothermics.2009.12.002.

Jóhannesson, H., 2009. Geological Map of Iceland – Bedrock Geology – 1:600,000. 1st edition.

Jóhannesson, T., Björnsson, H., Pálsson, F., Sigurðsson, O., Þorsteinsson, Þ., 2003. LiDAR mapping of the Snæfellsjökull ice cap, western Iceland. Jökull, 19–32.

Kohlstedt, D.L., Zimmerman, M.E., 1996. Rheology of partially molten mantle rocks. Annu. Rev. Earth Planet. Sci. 24, 41–62. http://dx.doi.org/10.1146/annurev.earth.24.1.41.

Kokfelt, T.F., Hoernle, K., Lundstrom, C., Hauff, F., van den Bogaard, C., 2009. Time-scales for magmatic differentiation at the Snæfellsjökull central volcano, western Iceland: constraints from U–Th–Pa–Ra disequilibria in post-glacial lavas. Geochim. Cosmochim. Acta 73, 1120–1144. http://dx.doi.org/10.1016/j.gca.2008.11.021.

Lister, J., Kerr, R., 1991. Fluid-mechanical models of crack propagation and their application to magma transport in dykes. J. Geophys. Res. 96, 10,049–10,077. http://dx.doi.org/10.1029/91JB00600.

Manconi, A., Longpe, M.A., Walter, T.R., Troll, V.R., Hansteen, T.H., 2009. The effects of flank collapses on volcano plumbing systems. Geology 37, 1099–1102. http://dx.doi.org/10.1130/G30104A.1.

McGuire, W.J., Howarth, R.J., Firth, C.R., Solow, A.R., Pullen, A.D., Saunders, S.J., Stewart, I.S., VitaFinzi, C., Vita-Finzi, C., 1997. Correlation between rate of sea-level change and frequency of explosive volcanism in the Mediterranean. Nature 389, 473–476. http://dx.doi.org/10.1038/38998.

McLeod, P., Tait, S., 1999. The growth of dykes from magma chambers. J. Volcanol. Geotherm. Res. 92, 231–246. http://dx.doi.org/10.1016/S0377-0273(99)00053-0.

Melnik, O., Sparks, R.S.J., 2005. Controls on conduit magma flow dynamics during lava dome building eruptions. J. Geophys. Res. 110, B02209. http://dx.doi.org/10.1029/2004JB003183.

Nakada, M., Yokose, H., 1992. Ice age as a trigger of active Quaternary volcanism and tectonism. Tectonophysics 212, 321–329. http://dx.doi.org/10.1016/0040-1951(92)90298-K.

Obermann, A., Lupi, M., Mordret, A., Jakobsdóttir, S.S., Miller, S.A., 2016. 3D-ambient noise Rayleigh wave tomography of Snæfellsjökull volcano, Iceland. J. Volcanol. Geotherm. Res. 317, 42–52. http://dx.doi.org/10.1016/j.jvolgeores.2016.02.013.

Pagli, C., Sigmundsson, F., 2008. Will present day glacier retreat increase volcanic activity? Stress induced by recent glacier retreat and its effect on magmatism at the Vatnajökull ice cap, Iceland. Geophys. Res. Lett. 35, 3–7. http://dx.doi.org/10.1029/2008GL033510.

Paquet, J., Francois, P., Nedelec, A., 1981. Effect of partial melting on rock deformation: experimental and natural evidences on rocks of granitic compositions. Tectonophysics 78, 545–565. http://dx.doi.org/10.1016/0040-1951(81)90028-7.

Parks, M.M., Moore, J.D.P., Papanikolaou, X., Biggs, J., Mather, T.A., Pyle, D.M., Raptakis, C., Paradissis, D., Hooper, A., Parsons, B., Nomikou, P., 2015. From quiescence to unrest: 20 years of satellite geodetic measurements at Santorini volcano, Greece. J. Geophys. Res., Solid Earth, 1309–1328. http://dx.doi.org/10.1002/2014JB0115.

Paterson, M.S., Wong, T.-F., 2005. Experimental Rock Deformation – The Brittle Field. Springer.

Pinel, V., Albino, F., 2013. Consequences of volcano sector collapse on magmatic storage zones: insights from numerical modeling. J. Volcanol. Geotherm. Res. 252, 29–37. http://dx.doi.org/10.1016/j.jvolgeores.2012.11.009.

Robock, A., 2000. Volcanic eruptions and climate. Rev. Geophys. 38, 191–219. http://dx.doi.org/10.1029/1998RG000054.

Rubin, A.M., 1995. Propagation of magma-filled cracks. Annu. Rev. Earth Planet. Sci. 23, 287–336. http://dx.doi.org/10.1007/s13398-014-0173-7.2.

Schmidt, P., Lund, B., Hieronymus, C., Maclennan, J., Árnadóttir, T., Pagli, C., 2013. Effects of present-day deglaciation in Iceland on mantle melt production rates. J. Geophys. Res., Solid Earth 118, 3366–3379. http://dx.doi.org/10.1002/jgrb.50273.

Scott, S., Driesner, T., Weis, P., 2015. Geologic controls on supercritical geothermal resources above magmatic intrusions. Nat. Commun. 6, 7837. http://dx.doi.org/10.1038/ncomms8837.

Sigmundsson, F., Pinel, V., Lund, B., Albino, F., Pagli, C., Geirsson, H., Sturkell, E., 2010. Climate effects on volcanism: influence on magmatic systems of loading and unloading from ice mass variations, with examples from Iceland. Philos. Trans. R. Soc. A, Math. Phys. Eng. Sci. 368, 2519–2534. http://dx.doi.org/10.1098/rsta.2010.0042.

Smith, R., Sammonds, P.R., Kilburn, C.R.J., 2009. Fracturing of volcanic systems: experimental insights into pre-eruptive conditions. Earth Planet. Sci. Lett. 280, 211–219. http://dx.doi.org/10.1016/j.epsl.2009.01.032.

Stefansson, R., Gudmundsson, G.B., Halldorsson, P., 2008. Tjörnes fracture zone. New and old seismic evidences for the link between the North Iceland rift zone and the Mid-Atlantic ridge. Tectonophysics 447, 117–126. http://dx.doi.org/10.1016/j.tecto.2006.09.019.

Tait, S., Jaupart, C., Vergniolle, S., 1989. Pressure, gas content and eruption periodicity of a shallow, crystallising magma chamber. Earth Planet. Sci. Lett. 92, 107–123. http://dx.doi.org/10.1016/0012-821X(89)90025-3.

Tarkov, A.P., Vavakin, V.V., 1982. Poisson's ratio behaviour in various crystalline rocks: application to the study of the Earth's interior. Phys. Earth Planet. In-

ter. 29, 24–29. http://dx.doi.org/10.1016/0031-9201(82)90134-0.
Tibaldi, A., Bonali, F.L., Pasquaré, F.A., Rust, D., Cavallo, A., D'Urso, A., 2013. Structure of regional dykes and local cone sheets in the Midhyrna–Lysuskard area, Snaefellsnes Peninsula (NW Iceland). Bull. Volcanol. 75, 1–16. http://dx.doi.org/10.1007/s00445-013-0764-8.
Tuitz, C., Exner, U., Frehner, M., Grasemann, B., 2012. The impact of ellipsoidal particle shape on pebble breakage in gravel. Int. J. Rock Mech. Min. Sci. 54, 70–79. http://dx.doi.org/10.1016/j.ijrmms.2012.05.018.
Violay, M., Gibert, B., Mainprice, D., Evans, B., Dautria, J.M., Azais, P., Pezard, P., 2012. An experimental study of the brittle–ductile transition of basalt at oceanic crust pressure and temperature conditions. J. Geophys. Res., Solid Earth 117, 1–23. http://dx.doi.org/10.1029/2011JB008884.
Violay, M., Gibert, B., Mainprice, D., Burg, J.-P., 2015. Brittle versus ductile deformation as the main control of the deep fluid circulation in oceanic crust. Geophys. Res. Lett. 42, 2767–2773. http://dx.doi.org/10.1002/2015GL063437.
Walter, T., Amelung, F., 2007. Volcanic eruptions following $M \geq 9$ megathrust earthquakes: implications for the Sumatra–Andaman volcanoes. Geology.
Watt, S.F.L., Pyle, D.M., Mather, T.A., 2013. The volcanic response to deglaciation: evidence from glaciated arcs and a reassessment of global eruption records. Earth-Sci. Rev. 122, 77–102. http://dx.doi.org/10.1016/j.earscirev.2013.03.007.
Zhong, X., Frehner, M., Kunze, K., Zappone, A., 2014. A novel EBSD-based finite-element wave propagation model for investigating seismic anisotropy: application to Finero Peridotite, Ivrea-Verbano Zone, Northern Italy. Geophys. Res. Lett. 41, 7105–7114. http://dx.doi.org/10.1002/2014GL060490.